HIGH-Q CAVITY OPERATION: STUDY ON THE THERMOELECTRICALLY INDUCED CONTRIBUTION TO RF SURFACE RESISTANCE

J.M. Vogt, A. Neumann, J. Knobloch, O. Kugeler, A. Velez, Helmholtz-Zentrum Berlin, Germany

Abstract

We present a study concerning the operation of a superconducting RF cavity (non-doped niobium) in horizontal testing with the focus on understanding the thermoelectrically induced contribution to the surface resistance. Starting in 2009, we suggested a means of reducing the residual resistance by warming up a cavity after initial cooldown to about 20 K and cooling it down again [1]. In subsequent studies we used this technique to manipulate the residual resistance by more than a factor of 2 [2]. We postulated that thermocurrents during cooldown generate additional trapped magnetic flux that impacts the cavity quality factor. Since several questions remained open, we present here a more extensive study including measurement of two additional passband modes of the 9-cell cavity that confirms the effect. We also discuss simulations that substantiate the claim. While the layout of the cavity LHe tank system is cylindrically symmetric, we show that the temperature dependence of the material parameters result in a non-symmetric current distribution. Hence a significant amount of magnetic flux can be generated at the RF surface resulting in an increased surface resistance [3].

SETUP

A fully equipped TESLA-type cavity welded into a titanium tank and with a TTF-3 input coupler installed was mounted horizontally inside the HoBiCaT [4] cryostat. The TESLA-type cavity reported on here received a heavy BCP (about 150 µm) prior to a 2 h bakeout at 800°C (no N_2 anneal). A light BCP etch followed the heat treatment. Before the helium tank was welded onto the cavity a quality factor of about $2{\cdot}10^{10}$ in the π mode at 2K was measured in a vertical test which corresponds to a residual resistance R_{res} of 1.2 nΩ if one assumes that the BCS resistance R_{BCS} did not change between vertical and horizontal test (fitting parameters for R_{BCS} in horizontal test are listed below).

The cavity was equipped with Cernox sensors on the helium vessel head and beam pipes near the Nb-Ti joints. Furthermore two heaters were attached, one on each beam pipe. The setup including the helium supply is sketched in Figure 1.

HoBiCaT can cool the cavity with different schemes. The cryoplant fills the helium via the filling line at the bottom left and/or the 2-phase-pipe from the top right. As discussed below, we used three different cooling schemes: The initial cooldown, the thermal cycle and the parked cooldown.

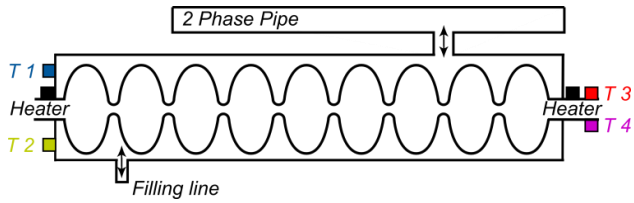

Figure 1: TESLA cavity in the LHe tank and equipped with four Cernox sensors and two heaters. The tank can be filled via the filling line and via the two phase pipe.

During the initial cooldown (whose temperature profile is shown in Figure 2a), the cavity is filled mainly via the filling line which creates a temperature gradient from its left to its right and from bottom to top. For a subsequent thermal cycle (Figure 2b), the cavity was filled via the 2-phase-pipe while the heaters were used to create a temperature difference between the cavity ends if desired. The targeted difference could be adjusted by varying the heater power. Values chosen were typical of those encountered during normal cooldowns. The "parked cooldown" (Figure 2c) from room temperature combines properties of both the initial cooldown and the thermal cycle. The cooling procedure of the initial cooldown was adapted to stop well before the sc phase transition. The cryoplant was balanced to maintain a constant temperature for 48 h. The set point was first set to 30K and then continuously lowered to 14K during this period. After all temperature sensors were clearly in equilibrium the set point was further lowered towards 1.8K and the cavity tank system transitioned with a small $\Delta T < 10$ K into the sc state.

THERMOELECTRIC EFFECT IN THE CAVITY HELIUM TANK SYSTEM

With the described setup, we investigated the hypothesis that thermoelectrically induced currents and their associated magnetic flux is responsible for the change of R_s upon thermal cycling. In the horizontal setup, the system is fabricated of two materials: Niobium (cavity) and titanium (helium tank) which create bimetal junctions. If a temperature difference is applied along the system (from left to right), a current is driven along the cavity and back through the tank. The additional temperature difference from bottom to top breaks the cylindrical symmetry of the system because the dc resistance of Nb and Ti is temperature dependent. Thus, even though mechanically the system is symmetric, the current is not and a magnetic field can be generated at the RF surface and get trapped during sc phase transition.

ISBN 978-3-95450-168-7

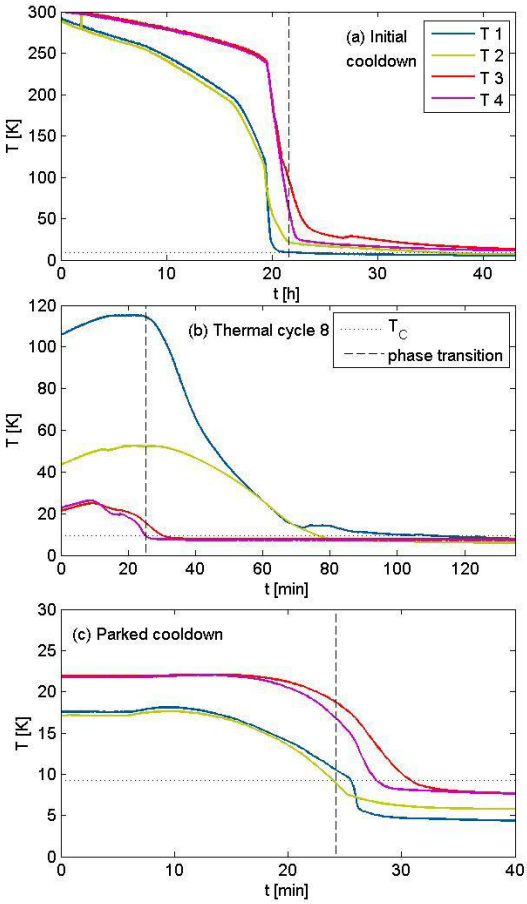

Figure 2: Temperatures measured during initial cooldown (a), a thermal cycle (b) and parked cooldown (c). The dotted line indicates T_c (9.2 K). The dashed line indicates the time when the first sensor dropped below T_c.

RF MEASUREMENTS

For the evaluation of the residual resistance in the nine cells of the cavity we measured the quality factor Q0 in three different passband modes: The π mode (1299MHz), the 8/9π mode (1298MHz) and the 1/9π mode (1274MHz). Each measurement is therefore an average over the cells which are exposed to the RF field in the respective mode ($\langle R_s \rangle = G/Q_0$). The geometry factor is taken from CST simulations: G_π = 271.2, $G_{8\pi/9}$ = 271.5, $G_{\pi/9}$ = 268.3.The π mode exhibits an equal field in each cell. The 1/9π mode has the maximum field in the center cells and low field in both end cells whereas the 8/9π mode has minimum field in the mid cell and maximum field in the end cells. We validated the theoretical field distribution in the cavity with a bead pull measurement after all RF measurements were completed.

We were able to distinguish between end cell region (dominant in 8/9π) and mid cell region (dominant in 1/9π) but we could not determine the cell number because all modes are mirrorsymmetric with respect to the cavity center plane in the axial direction. The RF measurements versus temperature confirmed that R_{BCS} did not vary between the three modes.

Table 1: Examples of Measured Residual Resistances of the Three Passband Modes

$R_{BCS} \approx 0.9n\Omega$ at 1.5 K	R_{res} π mode	8/9 π m.	1/9 π m.
Ini. cooldown	13.6	14.2	10.6
Cycle 8 (high ΔT)	13.3	18.6	8.0
Parked cooldown	6.4	9.9	1.4
Cycle 7 (low ΔT)	6.5	9.9	1.9

The fit of the data yielded: $R_S(T) = A \cdot \exp(-B/T) + R_{res}$ with A = (31.8 ± 2.2) μΩ and B = (15.7 ± 0.2) K. In contrast to R_{BCS}, the measured R_{res} was influenced by localized contributions like the spatial variation of HoBiCaTs ambient magnetic flux due to inhomogeneous shielding at the end cells. A higher surface resistance in the end cells lead to a lower Q in the 8/9π and π mode than in the 1/9π mode.

RESULTS

Table 1 provides examples of the measured residual resistances. We observed that cooldowns with a low temperature difference along the cavity result in lowest residual resistances. For the 1/9π mode this amounted to a residual resistance of 1.4 nΩ. Presumably the quality factor then is dominated by the ambient field in HoBiCaT which is about 0.2 - 0.5 μT along the center cells causing a residual resistance of 0.7 - 1.75 nΩ (assuming 1μT trapped flux causes 3.5nΩ additional R_s [5]). Other, non-flux, contributions may also add to the residual resistance.

Figure 3 displays the extracted residual resistances for all cooldowns and cycles as a function of temperature difference ΔT which is defined as: $|\Delta T| = |(T1+T2)/2 - (T3+T4)/2|$. The ΔT between the two ends of the tank is relevant for the thermocontact voltages. It is a measure for the induced thermoel. current and calculated at the instance when the first of the four sensors drops below T_c.

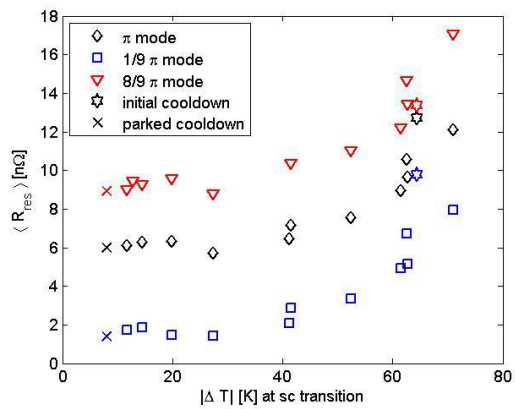

Figure 3: R_{res} measured with the three passband modes as a function of ΔT along the cavity at the onset of sc phase transition. The lowest R_{res} was achieved in the center cells following the cycle 1 and the parked cooldown (1.4 nΩ ≙ $Q_0 > 10^{11}$ at 1.5 K).

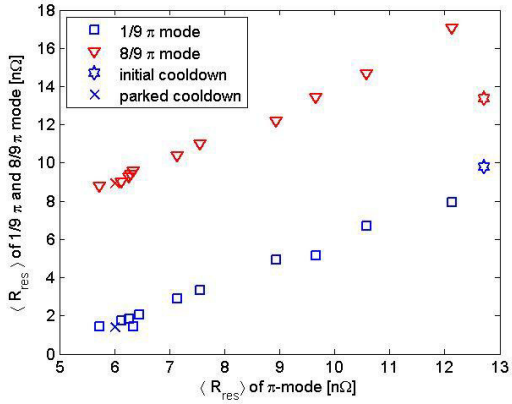

Figure 4: R_{res} obtained for the 8/9π and 1/9π mode as a function of R_{res} obtained for the π mode. Linear regression leaving out the initial cooldown results in: $R_{8/9\pi} = 1.2 \cdot R_{\pi} + 1.8$ nΩ and $R_{1/9\pi} = 1.0 \cdot R_{\pi} - 4.7$ nΩ.

Figure 3 shows that the residual resistance of the cavity decreases with decreasing ΔT. The curves for the three passband modes run parallel indicating that all nine cells are similarly affected. Thus the change in R_{res} is a global effect consistent with the thermocurrent model. Furthermore, we see that the 1/9π mode has a significantly reduced surface resistance compared to the two other modes while the residual resistance of the 8/9 π mode is elevated. We believe this is due to an increased ambient field in HoBiCaT near the end cells. Measurements of the magnetic shielding in HoBiCaT yielded that the magnetic field inside the end parts of the shield is increased due to cut outs for coupler and geometry effects (up to about 1 μT) [4].

Figure 4 compares the average surface resistance of the modes to that of the π mode. A linear dependency is visible for the cycles and the parked cooldown. The initial cooldown for the 8/9π mode does not fit into the linear curve which is already visible in Figure 3. This might be explained by the fact that the cooling dynamics of initial cooldown are different from the other cycles. Leaving out the data point of the initial cooldown, the two graphs in Figure 4 exhibit a linear behavior. The slopes are 1.2 (8/9π mode) and 1.0 (1/9π mode) which is close to 1 meaning that all cells are affected by the thermocurrent in a similar way.

To investigate the experimental results further and to make a quantitative analysis of the thermocurrents we performed sample measurements of the thermopower on niobium (RRR = 300) and titanium (grade 2) and, based on the acquired data, we turned to numerical simulations of a simplified system using COMSOL [3]. In particular it was important to understand the spatial distribution of the currents and the magnetic flux.

Figure 5 displays the thermoelectrically induced magnetic field on the RF surface that was calculated in our simplified COMSOL simulations compared to the RF measurements in the 1/9π mode. The results show that the magnetic field increases with the temperature difference.

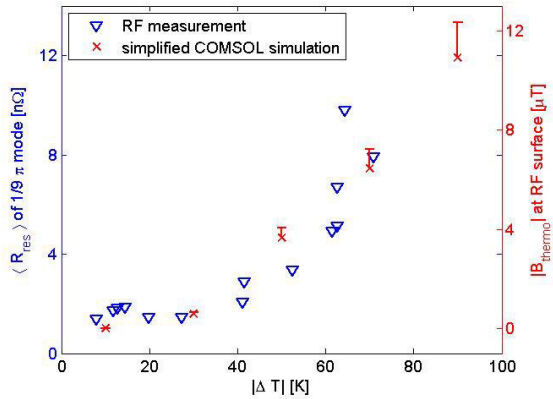

Figure 5: Magnetic field at the RF surface simulated for different temperature differences in combination with the RF data of Figure 3. The red bars indicate the magnetic field that is obtained assuming a 30% higher thermopower, corresponding roughly to the uncertainty in our measurement of the Nb thermopower [3].

While we do not claim that the quantitative values should be directly compared, the trend is very similar.

CONCLUSION

We demonstrated that poorly controlled cooling conditions can significantly deteriorate the quality factor of SRF cavities due to the generation of thermocurrents. We also demonstrated that an initial cooldown through T_c with reduced ΔT can in principle yield residual resistances at 1 nΩ, provided the external magnetic shielding is very effective in eliminating external residual flux. The observations are in agreement with COMSOL simulations [3].

What we did not investigate here is the influence of changed cooling conditions on the efficacy of the Meissner effect since our magnetic shield eliminated most of the residual external field.

ACKNOWLEDGMENT

We would like to thank our engineers Michael Schuster, Andre Frahm, Sascha Klauke, Dirk Pflückhahn, Stefan Rotterdam and Axel Hellwig for experimental support.

REFERENCES

[1] O. Kugeler, et. al., SRF2009, 352 (2009).
[2] J. M. Vogt, O. Kugeler and J. Knobloch, Phys. Rev. ST Accel. Beams 16, 102002 (2013).
[3] J. M. Vogt, O. Kugeler and J. Knobloch, Phys. Rev. ST Accel. Beams 18, 042001 (2015).
[4] O. Kugeler, A. Neumann, W. Anders, and J. Knobloch, Review of Scientific Instruments 81, 074701 (2010).
[5] B. Aune et al., Phys. Rev. ST Accel. Beams 3, 092001 (2000).

ISBN 978-3-95450-168-7